Journal of Power Sources 193 (2009) 400–407

Contents lists available at ScienceDirect

Journal of Power Sources

journal homepage: www.elsevier.com/locate/jpowsour

Zirconium doping effect on the performance of proton-conducting $BaZr_yCe_{0.8-y}Y_{0.2}O_{3-\delta}$ ($0.0 \le y \le 0.8$) for fuel cell applications

Youmin Guo, Ye Lin, Ran Ran, Zongping Shao*

State Key Laboratory of Materials-Oriented Chemical Engineering, College of Chemistry & Chemical Engineering, Nanjing University of Technology, No.5 Xin Mofan Road, Nanjing 210009, PR China

ARTICLE INFO

Article history:
Received 26 February 2009
Received in revised form 24 March 2009
Accepted 25 March 2009
Available online 2 April 2009

Keywords:
Proton
$BaZr_yCe_{0.8-y}Y_{0.2}O_{3-\delta}$
CO_2-TPD
Solid oxide fuel cells

ABSTRACT

High-temperature proton conductors are promising electrolytes for protonic solid oxide fuel cells (H^+-SOFCs). In this study, the relationship between the Zr doping content and structure, chemical stability, carbon dioxide resistivity, sinterability and electrochemical properties of $BaZr_yCe_{0.8-y}Y_{0.2}O_{3-\delta}$ (BZCYy), $0.0 \le y \le 0.8$, are studied systemically using XRD, CO_2-TPD, SEM, EIS and I–V polarization characterizations. Zr doping suppresses carbonate formation, CO_2-TPD demonstrates that the formative rate of carbonate over BZCYy are 7.50×10^{-6} and 8.70×10^{-7} mol m^{-2} min^{-1} at $y = 0.0$ and 0.4, respectively. Investigation of sinterability shows that the anode-supported configuration helps the sintering of the thin-film electrolyte. Peak power densities of 220 and 84 mW cm^{-2} are obtained at 750 and 450 °C, respectively, with BZCY0.4 electrolyte. Due to the favorable chemical stability against CO_2 and good sintering in the thin-film configuration, BZCY0.4 is a potential electrolyte material for H^+-SOFCs.

1. Introduction

During the past decades, solid oxide fuel cells (SOFCs) have gained considerable attention as advanced power generation devices because of their high-energy conversion efficiency, low environmental impact and good fuel flexibility [1–3]. Traditional SOFCs are composed of yttria-stabilized zirconia electrolytes and operate at approximately 1000 °C. Although such a high operating temperature is beneficial for promoting the electrode reactions and ensures sufficient ionic mobility inside the electrolyte, it also introduces a series of problems such as fast sintering of electrodes, high reactivity between cell components and expensive interconnecting materials. Consequently, there is increasing interest in reducing the operating temperature of SOFCs to the intermediate-temperature range, i.e. 400–800 °C [4–7], thereby allowing a more flexible choice of cell materials and prolonging the lifetime of the device.

Up to now, the most applied SOFC electrolytes have been oxygen-ionic conducting oxides including yttria or scandia stabilized zirconia, or gadolinia or samaria doped ceria. Due to the large size of the ion, the activation energy (E_a) for oxygen ion diffusion reaches approximately 0.8 eV [8,9]. Consequently, a quick drop in ionic conductivity with reducing operating temperature is normally observed for many O^{2-} conductors. Iwahara et al. first demonstrated that some perovskite-type oxides exhibited proton conduction at elevated temperatures under a humidified atmosphere [10,11]. A proton moves much more easily than an oxygen ion because of its much smaller ionic size, consequently a lower E_a of 0.3–0.6 eV is typically observed [9,12]. Thereby, proton-conducting oxides are superior to oxygen-ion conducting oxides for reduced temperature operation.

Today, there is a tremendous interest in the research and application of proton-conducting oxides for use as electrolytes for fuel cells and electrolyzers [13–15]. At present, high-temperature proton conductors are reported for several perovskite-structure oxides, such as doped $BaCeO_3$, $SrCeO_3$, $BaZrO_3$ and $SrZrO_3$ [16]. Although some discrepancies still existed in the literatures, yttrium-doped $BaCeO_3$ ceramics are generally believed to possess the highest protonic conductance when compared to the others and may even exceed that of the well-known high oxygen-ionic conducting oxides of doped ceria at temperatures lower than 600 °C [17], making them highly promising as electrolytes of IT-SOFCs. However, such materials were found to be unstable under water vapor and carbon dioxide atmospheres [18,19]. They can react with acidic gases, such as CO_2, and moisture resulting in destruction of the perovskite structure [20–22]. Therefore, developing new proton-conducting materials with adequate protonic conductivity as well as good chemical stability over the range of IT-SOFCs, operating conditions has become a practical challenge.

Considerable research efforts have focused on tailoring the phase stability and conductivity of proton conductors via doping [12,18–20,23–28]. $BaZrO_3$ has a similar lattice structure to $BaCeO_3$, and possesses sufficiently high stability to water and carbon

* Corresponding author. Tel.: +86 25 83172256; fax: +86 25 83172256.
E-mail address: shaozp@njut.edu.cn (Z. Shao).

0378-7753/$ – see front matter © 2009 Elsevier B.V. All rights reserved.
doi:10.1016/j.jpowsour.2009.03.044

dioxide but poor protonic conductivity and poor sinterability [29–31]. The formation of a $BaCeO_3$ and $BaZrO_3$ solid solution may result in a balance between the chemical stability, sinterability and protonic conductivity. Zhong studied the stability and conductivity of the $BaCe_{0.9-x}Zr_xY_{0.1}O_{2.95}$ series and found that the chemical stability increased while the electric conductivities of sintered samples decreased with the Zr content [23]. The optimal zirconium content was found to be around $y = 0.4$. The electrical conductivity and the chemical stability of $BaCe_{0.9-x}Zr_xY_{0.1}O_{3-\delta}$ systems have also been investigated by Katahira et al. [20], who came to similar conclusions. The phase stability and protonic conductivity of $BaZr_{0.1}Ce_{0.7}Y_{0.2}O_{3-\delta}$, a specific composition among the $BaCe_{0.8-y}Zr_yY_{0.2}O_{3-\delta}$ series, was investigated by Zuo et al. An air|H_2 fuel cell with a 65 μm thick $BaZr_{0.1}Ce_{0.7}Y_{0.2}O_{3-\delta}$ electrolyte was fabricated and delivered attractive open circuit voltages of 1.01 and 1.05 V and peak power densities of 148 and 56 mW cm^{-2} at 600 and 500 °C, respectively [19]. However, later experiments showed that $BaZr_{0.1}Ce_{0.7}Y_{0.2}O_{3-\delta}$ may still have insufficient stability under a reforming gas atmosphere. Fabbri et al. investigated the effect of the Zr doping amount on the sintering, CO_2 resistivity and fuel cell performance of $BaCe_{0.8-y}Zr_yY_{0.2}O_{2.95}$ [12]. The optimal Zr doping content was found to around $y = 0.5$. A thick $BaZr_{0.5}Ce_{0.3}Y_{0.2}O_{3-\delta}$ electrolyte-supported cell sintered at 1550 °C for 8 h with Pt electrodes delivered a peak power density of only 18 mW cm^{-2} at 700 °C. It was found there was a synergetic effect between the electrode and electrolyte.

In this work, we reported a systemic study of the relationship between the Zr doping content and the structure, chemical stability, carbon dioxide resistivity, sinterability and electrochemical properties of $BaZr_yCe_{0.8-y}Y_{0.2}O_{3-\delta}$ (BZCYy), $0.0 \le y \le 0.8$, by X-ray diffraction (XRD), CO_2-temperature-programmed desorption (CO_2-TPD), scanning electron microscopy (SEM), electrochemical impedance spectroscopy (EIS) and *I–V* polarization characterizations. An anode-supported thin-film electrolyte configuration was specifically adopted in this study. Effects of the electrolyte configuration on the sintering behavior were studied.

2. Experimental

2.1. Synthesis and fabrication

$Ba_{0.5}Sr_{0.5}Co_{0.8}Fe_{0.2}O_{3-\delta}$ (BSCF) perovskite oxide was adopted as the cathode. Both BSCF and $BaZr_yCe_{0.8-y}Y_{0.2}O_{3-\delta}$ (BZCYy, $0.0 \le y \le 0.8$) oxide powders were prepared by an EDTA–citrate complexing sol–gel process that uses analytic grade metal nitrates $Ba(NO_3)_2$, $Zr(NO_3)_4{\cdot}5H_2O$, $Sr(NO_3)_2$, $Ce(NO_3)_3{\cdot}6H_2O$ and $Y(NO_3)_3{\cdot}6H_2O$ as raw materials. Taking the preparation of $BaZr_{0.1}Ce_{0.7}Y_{0.2}O_{3-\delta}$ (BZCY0.1) as an example, the required amounts of metal nitrates were mixed in solution state, and EDTA and citric acid were then added to serve as the complexing agents with the molar ratio of total metal ions to EDTA to citric acid set at 1:1:2. The pH value of the solution was adjusted to around 6 using NH_4OH and the water was evaporated at 90 °C until transparent gels, were formed. These were pre-treated at 240 °C to remove most of the organics and then calcined at 900–1000 °C for 5 h under an air atmosphere to obtain the products with the desired lattice structure.

For sintering investigation, the powders with varied zirconium doping content calcined from 1000 °C were uniaxially pressed into cylindrical shape pellets (15 mm in diameter) at about 300 MPa and then sintered in air at 1500 °C for 5 h. For fuel cell performance investigation, anode-supported cells with BZCYy ($y = 0.0$, 0.4 and 0.8) electrolytes were prepared using a co-pressing technique. Anode powders consisting of 60 wt.% NiO and 40 wt.% BZCYy were prepared by mixing NiO and BZCYy with an agate mortar. To fabricate the single cell, the well-mixed NiO + BZCYy powders were dropped into a stainless steel die with a diameter of 15 mm and pressed as a substrate. BZCYy powder (about 0.03 g) was then distributed over the top of the substrate and pressed again to form a bilayer pellet, which was fired under stagnant air at 1450 °C for 5 h to make the densification of the electrolyte layer. The BSCF slurry was prepared by dispersing BSCF powder into a mixed solution of glycerol, isopropyl alcohol and ethylene glycol using high-energy ball milling (Fritsch Pulverisettle 6) at the rotation rate of 400 rpm for 40 min. This slurry was then painted on the central surface of the electrolyte. The triple-layered cell was fired at 1000 °C for 2 h in air. The resulted coin-shape cathode had an effective area of 0.48 cm^2.

2.2. Single-cell test

The cell performance was tested over a home-built fuel cell test station. The cell was sealed onto a quartz tube using silver paste as the sealing material. Three percent H_2O humidified H_2 at a flow rate of 40 ml min^{-1} and controlled by a mass flow controller (standard temperature pressure, STP) was fed into the anode chamber as fuel, and ambient air was adopted as the cathode atmosphere. *I–V* polarization curves were collected using a digital electrometer (Model 2420, Keithley, USA) based on the four-probe configuration. The impedance spectroscopy of the cells were measured under an open circuit voltage (OCV) condition with a Solartron 1260A frequency response analyzer in combination with a Solartron 1287 potentiostat that was interfaced with a computer using the *Z*-plot software.

2.3. Other characterizations

The crystal structures of the synthesized powders and the pre-treated samples under a CO_2 atmosphere were determined using X-ray diffraction (Model D8 Advance, Bruker, Germany) with Cu Kα radiation. The experimental diffraction patterns were collected at room temperature by step scanning within the range of $20° \le 2\theta \le 90°$. The specific surface area of the synthesized powders was characterized by N_2 adsorption at the temperature of liquid nitrogen using a BELSORP II instrument. Prior to analysis, the samples were treated at 250 °C for 2 h in vacuum to remove the weakly adsorbed species on the surface. The microscopic features of the prepared electrolyte pellets and single cells were characterized using an environmental scanning electron microscope (ESEM; Model QUANTA-2000).

A carbon dioxide temperature-programmed desorption (CO_2-TPD) study of the samples pretreated with CO_2 atmosphere at 650 °C for 2 h was conducted in a home-constructed multipurpose temperature-programmed apparatus. The test was performed from 200 to 930 °C with a heating rate of 10 °C min^{-1}. Argon was used as the purge gas at a flow rate of 20 ml min^{-1} and the effluent gas was monitored by a mass spectrometer (MS; Model QIC-20, Hiden, UK). The amount of sample was approximately 150 mg. The amount of carbonate formed in the samples after the treatment in a CO_2 atmosphere were calculated from the areas of desorption peaks using $SrCO_3$ as the standard substance.

3. Results and discussion

3.1. Phase structure

The oxide powders with the nominal composition of $BaZr_yCe_{0.8-y}Y_{0.2}O_3$ ($y = 0.0$–0.8, 0.1 in step), calcined from 1000 °C in air and cooled down to room temperature naturally, were submitted for phase examination. As shown in Fig. 1a, all of the oxides show the phase-pure perovskite-type structure. The lattice symmetry of the oxides can be indexed as mainly monoclinic for

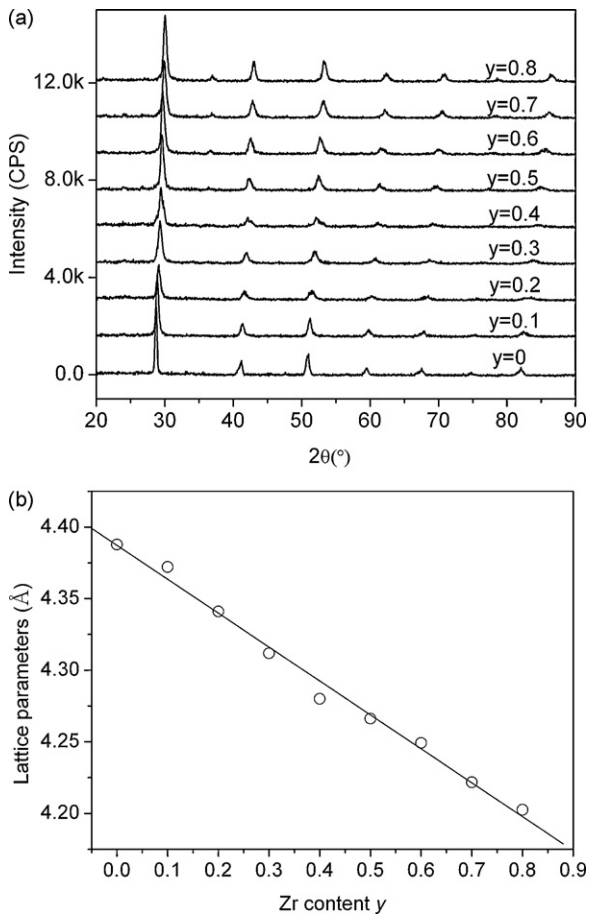

Fig. 1. (a) XRD patterns of the synthesized BZCYy ($0.0 \le y \le 0.8$) oxides with varied Zr content calcined at 900–1000 °C for 5 h, (b) lattice constants (Å) of the BZCYy ($0.0 \le y \le 0.8$) oxides with varied Zr content based on quasi-cubic lattice symmetry.

$y = 0.0$ ($BaCe_{0.8}Y_{0.2}O_3$), orthorhombic for $y = 0.1$–0.5, and cubic for $y = 0.6$, 0.7 and 0.8. The results agree well with those reported by Fabbri et al. [12]. To further demonstrate the formation of the solid solution over the whole range of Zr^{4+} doping content ($y = 0.0$–0.8), the lattice constants were determined from XRD analysis assuming quasi-cubic lattice symmetry and the results as shown in Fig. 1b. A progressive decrease of the lattice constant with increasing Zr concentration was observed. Such a phenomenon can be well explained by the fact that Zr^{4+} (0.72 Å) has a smaller ionic radius than Ce^{4+} (0.87 Å) at the B-site of perovskite in six coordination with oxygen ion. There were no superlattice diffractions indicating an ordering of Ce^{4+} and Zr^{4+} at the Ce^{4+}-site. From these results, we conclude that the Ce^{4+} and Zr^{4+} in BZCYy are likely randomly distributed in the lattice.

3.2. Chemical stability against CO_2 atmosphere

One obvious feature of SOFC is its capability to operate on carbon-containing fuel. This is a great advantage over low temperature polymer-electrolyte fuel cell since hydrocarbons fuel has a much better matured infrastructure than hydrogen fuel. Although SOFCs with proton-conducting electrolyte cannot directly convert hydrocarbon fuel into electrical power, the hydrocarbon can be reformed to CO_2 and H_2 in-situ under the catalyst of the anode. Because of the high concentration of CO_2 in the reforming gas, the electrolyte should possess sufficient chemical stability against CO_2. However, $BaCeO_3$-based proton conductors were found to have poor chemical stability under CO_2 and H_2O atmospheres [31]. Barium cerate can react with CO_2 and H_2O according to reaction (1) and (2), respectively,

$$BaCeO_3 + CO_2 \rightarrow BaCO_3 + CeO_2 \quad (1)$$

$$BaCeO_3 + H_2O \rightarrow Ba(OH)_2 + CeO_2 \quad (2)$$

It was reported that the increase of Zr concentration in $BaZr_yCe_{0.9-y}Y_{0.1}O_3$ resulted in increase in the chemical stability of the oxide against CO_2 [25]. In order to verify the chemical stability of $BaZr_yCe_{0.8-y}Y_{0.2}O_3$ in CO_2 atmosphere, the BZCYy powders with various Zr contents in the lattice were exposed to pure CO_2 in a tube furnace at 650 °C for 2 h and the phase composition of the specimens was investigated by room-temperature X-ray diffraction. Fig. 2 shows the corresponding XRD patterns of the powders after the CO_2 exposure. It was observed that the perovskite structure of BZCYy oxides was destroyed when the carbonate formed at $y \le 0.3$. This suggests that reaction (1) happened during the treatment of BZCYy ($y = 0.0$, 0.1, 0.2, 0.3) oxides in the CO_2 atmosphere. Thus, BZCYy with a low zirconium doping concentration ($y \le 0.3$) may not be applicable as an electrolyte for SOFC operating on a reforming gas. When the zirconium doping amount (y) reached 0.4, the main perovskite structure was survived although some diffraction peaks of carbonate were still observed. With the further increase of Zr doping concentration ($y \ge 0.4$), the relative intensity of perovskite increased while the peak intensity of carbonate decreased sharply. At $y = 0.8$, no carbonate diffraction peak was detected in the XRD diffraction pattern of the oxide after the CO_2 treatment. Similar phenomena were also observed by Fabbri et al. [12], who observed that the perovskite structure survived at $y = 0.5$ or higher after the BZCYy samples were treated in pure CO_2 at 900 °C for 3 h.

Our results are also consistent with some reports under similar experimental conditions [12,19,20,23]. However, X-ray diffraction is not a sufficiently precise tool for this analysis because of carbonate may exist in the amorphous state which is not detectable by XRD, the CO_2-TPD technique was applied to further determine the effect of Zr doping on the chemical stability against carbon dioxide. The oxide powders after the treatment in the CO_2 atmosphere were put into a U-type quartz tube reactor. After blowing away the weakly adsorbed impurities on the surface by an argon purge for about half an hour, the temperature of oxide powder was increased at 10 °C min^{-1} with the help of a temperature controller. Any carbonate formed over the oxide surface or in the bulk was thermally decomposed into gaseous carbon dioxide, which was carried out by the sweep gas argon to the on-line mass spectrometer (MS) for analysis of the CO_2 concentration. Fig. 3 shows the CO_2-TPD pro-

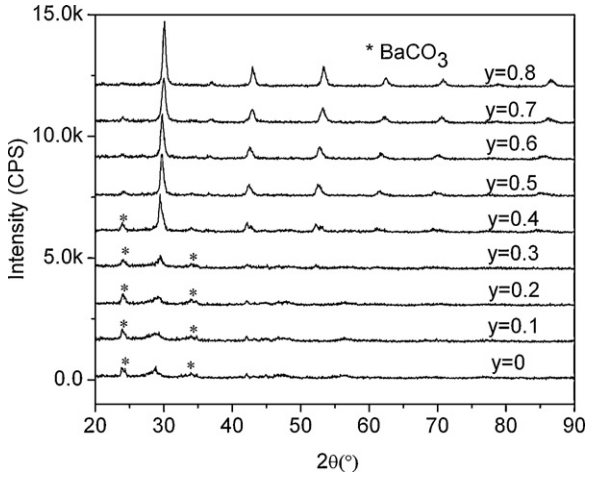

Fig. 2. XRD patterns of BZCYy ($0.0 \le y \le 0.8$) powders after treatment in a CO_2 atmosphere at 650 °C for 2 h.

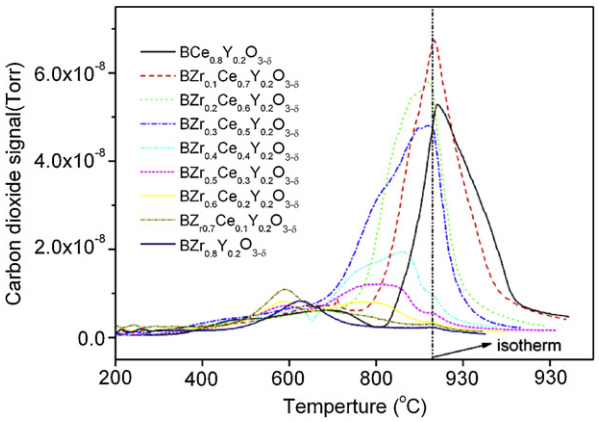

Fig. 3. CO_2-TPD profiles of the BZCYy oxides at various Zr content (y = 0.0–0.8).

files of the BZCYy (y = 0.0–0.8) oxides at various Zr content. Two kinds of CO_2 desorption peaks were observed for all samples with one peak around 600 °C (named as α desorption), and the other located between 800 and 930 °C (named as β desorption). They can be ascribed to the desorption of the surface-absorbed CO_2 and the decomposition of the bulk carbonate, respectively. It was observed that the BZCYy oxides had a very large β desorption peak at high temperature at y = 0.0, 0.1, 0.2 and 0.3. BZCY0.1 had an even bigger β desorption peak area than that of undoped BCY. When the zirconium content y reached 0.4, the desorption peak intensity decreased significantly, and the peak intensity decreased with a further increase of Zr content. With the increase of the zirconium content, the β desorption peak moved towards the lower temperature range. This suggests that the formation of carbonate becomes more difficult when there is more zirconium. In other words, the chemical stability of the oxide against CO_2 was improved as the Zr content increased, agreeing well with observations in the literature [21,23].

Since the solid–gas reaction occurred over the solid surface, the amount of carbonate is also closely related to the surface area of the oxide. The specific surface areas of the oxides with varying zirconium content were measured, and the results are listed in Table 1. They show that the surface area increased with increasing zirconium content, which is in agreement with the general observation of the suppressing effect of zirconium on the sintering of the oxide [32].

The area of the desorption peak reflects the amount of carbonate in BZCYy, which was quantitatively determined by applying pure $SrCO_3$ as an external standard substance. The area-specific carbonate formative rates over BZCYy at various Zr contents are also listed in Table 1. They clearly show that small amount of Zr doping efficiently suppressed the carbonate formation. When only 1/8 of the Ce site was substituted by Zr with the formation of BZCY0.1, the carbonate formative rate decreased more than three-fold. With the further increase of the zirconium doping amount the carbonation formative rate reduced monotonically. The formative rate of carbonate is 7.50×10^{-6} mol m^{-2} min^{-1} at y = 0.0 while it is only 7.00×10^{-8} mol m^{-2} min^{-1} at y = 0.8. Furthermore, there was almost no bulk carbonate formed at y = 0.8. The above results are in full agreement with the XRD results.

Table 1
BET and carbonate formative rate of the BZCYy ($0.0 \le y \le 0.8$) oxides at various Zr contents.

Zr content y	BET ($m^2\ g^{-1}$)	Carbonate formative rate (10^{-6} mol m^{-2} min^{-1})
0	1.6(1)	7.50
0.1	6.0(7)	2.07
0.2	6.8(7)	1.82
0.3	7.5(9)	1.54
0.4	6.5(5)	0.87
0.5	11.4(5)	0.36
0.6	14.1(3)	0.17
0.7	18.7(2)	0.11
0.8	20.8(9)	0.07

3.3. Sinterability

It was generally believed that the $BaZrO_3$-based oxides are much more difficult to sinter than the $BaCeO_3$-based perovskite oxides. Thus, the increase of zirconium content in BZCYy is believed to result in worse sinterability of the oxide. The increase of specific surface area with zirconium doping concentration as shown in Table 1 strongly supports this assumption. Typical SOFCs employ a nickel-based anode since nickel possesses high electronic conductivity, excellent catalytic activity for hydrogen electro catalytic oxidation, and also favorable activity for reforming of hydrocarbons to hydrogen. However, nickel oxide is also easily sintered at high temperature. The fuel cell electrode should have sufficient porosity to allow the free diffusion of gaseous reactants and products to minimize the concentration polarization. Thus, a sintering temperature of 1350–1450 °C is usually applied for the nickel-based anode. Such a sintering temperature ensures good connection between the anode particles and also maintains sufficient anode surface area and porosity for electrode reactions. In a previous study, high sintering temperatures above 1550 °C were applied for the densification of BZCYy electrolytes, especially for those with high zirconium doping contents [32]. Such high sintering temperatures may still be applicable for electrolyte-supported SOFCs since the electrolyte layer can be fabricated separately from the anode and cathode layers, although higher sintering temperature means higher fabrication costs. To reduce the electrolyte ohmic drop, a thin-film electrolyte configuration was applied in this study. To maintain sufficient mechanical strength, the thin electrolyte layer must be supported on a substrate. Nowadays, an anode-supported thin-film electrolyte configuration is usually applied, and this configuration was also adopted in this study. A co-firing of the anode–electrolyte dual-layer cell to densify the electrolyte layer is necessary in the fabrication of the anode-supported thin-film electrolyte SOFC. To avoid the sintering of the anode, the cell should be sintered at a temperature lower than 1500 °C. Therefore, a sintering temperature of 1500 °C was first adopted for the BZCYy electrolytes. The BZCYy powders were pressed into thick disk-shape pellets using a stainless steel die and sintered at 1500 °C in air for 5 h.

Fig. 4 shows the surface morphologies of the BZCYy (y = 0.0, 0.1 0.3, 0.4, 0.7, 0.8) electrolyte after sintering at 1500 °C. The BCY electrolyte was well densified, and very few enclosed pores were observed. With an increase in the Zr doping content, an increasing number of enclosed pores were observed. At y = 0.3, the electrolyte was still well densified. However, a considerable number of pores were observed inside the pellet at y = 0.4. At y = 0.7 and 0.8, the pellets were in highly porous state which was similar to the initial powder with a very fine grain size. Table 2 lists the linear shrinkage of the disk after the sintering and the relative density of the resulting pellets, calculated based on the volume of the pellet found by measuring the diameter, thickness and the weight, and using the theoretical density of the oxides. Table 2 clearly shows a monotonic decrease in sintering density with increasing Zr doping content. At y = 0.8, the relative density is only 65.67%. A similar suppressing effect of zirconium doping on the sintering of the electrolyte was reported in literature [33].

In the anode-supported thin-film electrolyte configuration, the anode and the electrolyte layers are co-fired at a high temperature, so the sintering behavior of the electrolyte layer may be affected

by the anode. Therefore, it is necessary to investigate the sintering behavior of the dual layer cells. The NiO + BZCY*y* anode-supported thin-film BZCY*y* dual-layer cells were fabricated by a dual drying pressing. The green dual-layer pellets were then co-fired at a high temperature. To ensure sufficient porosity of the anode layer, the co-firing temperature was reduced to 1450 °C. Shown in Fig. 5 are the cross sectional photos of the as-fabricated single cells with BZCY*y* electrolytes (y = 0.0, 0.3, 0.4 and 0.8) and the BSCF cathode (1000 °C fired). The electrolyte has a thickness of 25–40 μm. As compared to the self-supported thick BZCY*y* electrolytes, the thin-film electrolytes were much more densified at a high zirconium doping amount. Even with the BZCY0.8 electrolyte, no penetrated pores were observed although a large number of enclosed pores were still observed inside the electrolyte layer. This implies that the anode-supported configuration helped the sintering of the thin-film electrolyte.

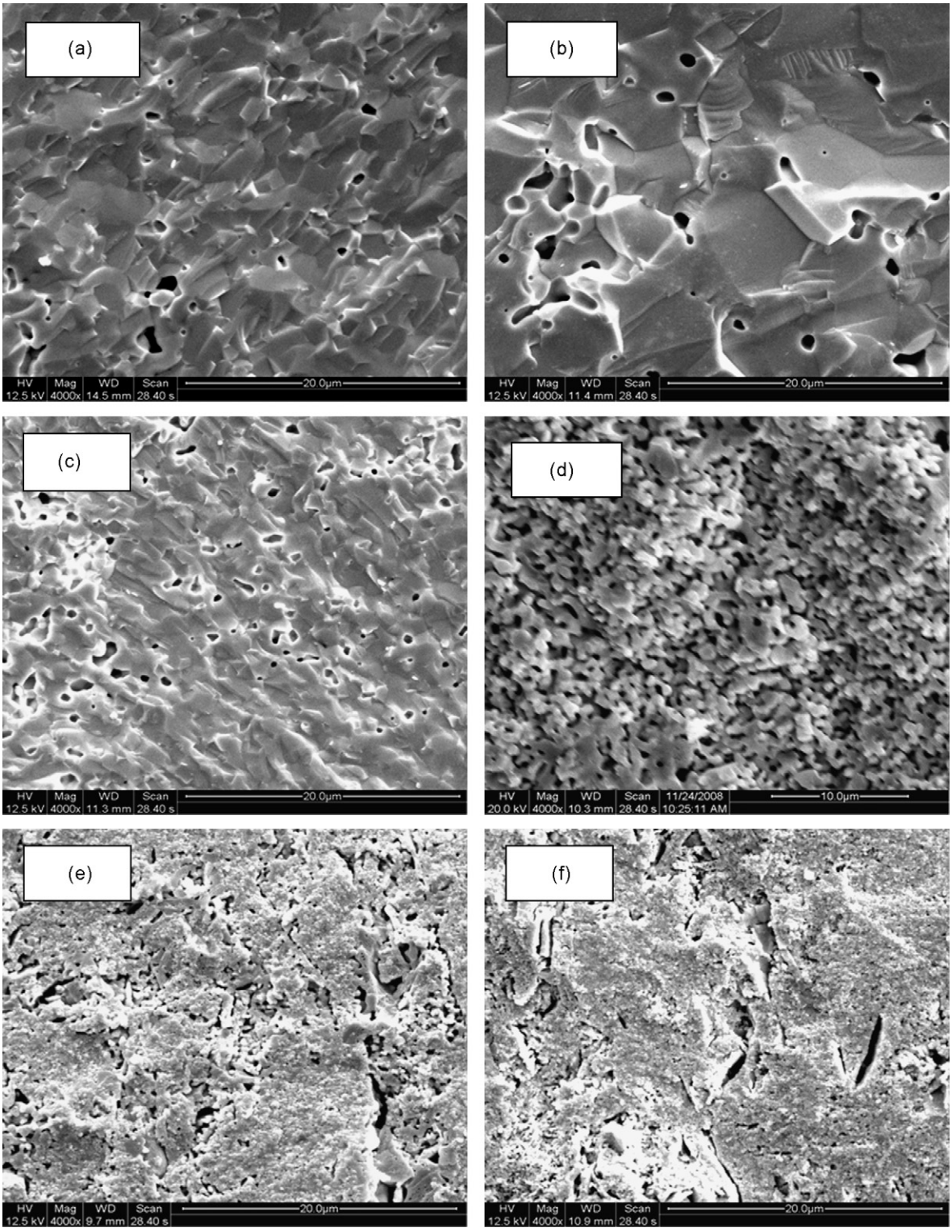

Fig. 4. Surface morphologies of the BZCY*y* electrolyte after sintering at 1500 °C: (a) y = 0.0; (b) y = 0.1; (c) y = 0.3; (d) y = 0.4; (e) y = 0.7; (f) y = 0.8.

Table 2
The comparison of the linear shrinkages for the self-supported (sintered at 1500 °C) and anode-supported (sintered at 1450 °C) BZCY*y*. The relative density of the BZCY*y* ($0.0 \le y \le 0.8$) pellets sintered at 1500 °C.

Zr content *y*	Linear shrinkage of self-supported BZCY*y* (%)	Linear shrinkage of anode-supported BZCY*y* (%)	Relative density (%)
0	15.33	15.45	92.29
0.1	15.06	15.12	91.36
0.2	14.67	–	89.93
0.3	14.27	14.85	88.70
0.4	13.01	13.73	84.89
0.5	12.40	–	82.94
0.6	11.27	12.97	80.46
0.7	10.27	–	76.34
0.8	8.33	11.99	65.67

The sintering of the thin-film electrolyte on the anode substrate is actually a constraint sintering process. Since the anode is about 0.6 mm which is more than 10 times that of the electrolyte thickness (25–40 μm), the anode has a greater impact on the sintering behavior of the thin-film electrolyte than the electrolyte has on the sintering of the anode. As shown in Table 2, the shrinkages of the anode after the sintering were 15.45%, 15.12%, 14.85%, 13.73%, 12.97% and 11.99% for $y = 0.0$, 0.1, 0.3, 0.4, 0.6 and 0.8, respectively, for the anode-supported dual-layer cells. As compared to the self-supported BZCYy, at lower zirconium doping content, i.e., $y = 0.0$ or 0.1, the electrolyte shrinkage is slightly bigger than for the self-supported thick BZCY*y* electrolyte. At high zirconium doping content, i.e., $y = 0.4$, 0.6 and 0.8, the shrinkage of the thin-film electrolyte was much larger than that of the self-supported thick BZCY*y* electrolyte. This then explained the relatively worse sintering of the thin-film BZCY electrolyte at low zirconium doping content than the sintering of the thin-film BZCY electrolyte at high zirconium doping content. At a high zirconium doping content, the large anode shrinkage allowed for better contact of the electrolyte BZCY*y* particles and accelerated the sintering of the thin-film electrolyte. This may be one of the important causes for the improved sintering of the thin-film electrolyte at high zirconium doping concentrations. The inter-diffusion of metal ions between the anode and electrolyte layers during the high temperature sintering may also facilitate the sintering of the electrolyte layer. It has been reported that nickel oxide is a sintering aid for the

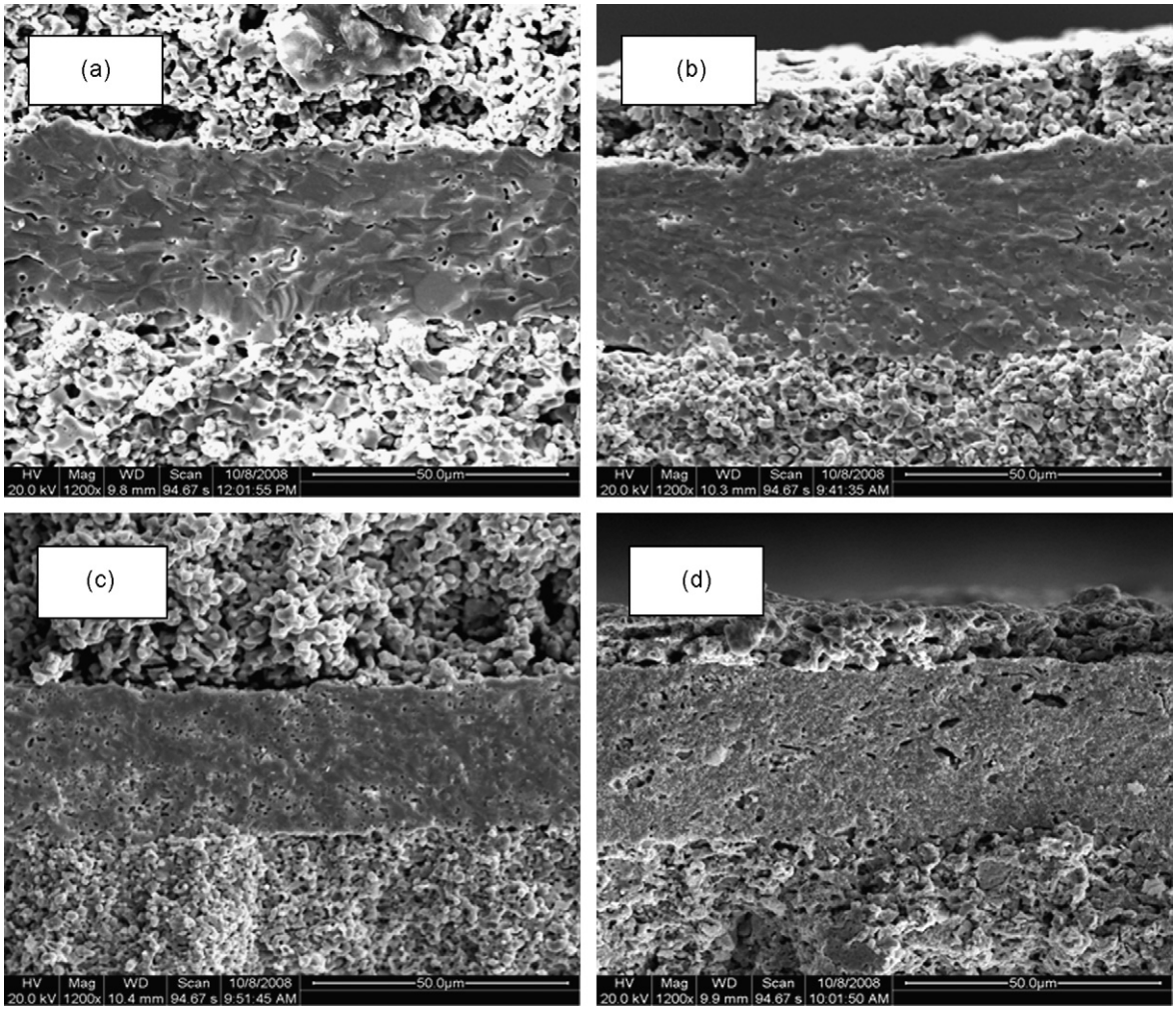

Fig. 5. Cross-sectional morphologies of the as fabricated single cells with BZCY*y* electrolytes and the BSCF cathode (1000 °C fired): (a) $y = 0.0$; (b) $y = 0.3$; (c) $y = 0.4$; (d) $y = 0.8$.

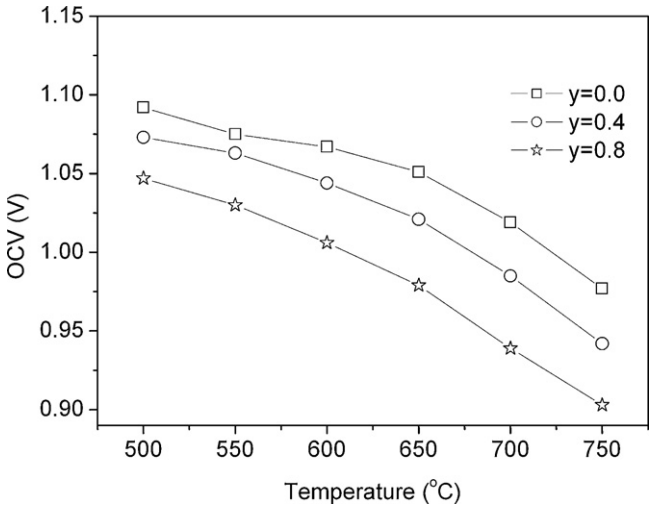

Fig. 6. Operating temperature dependence of open circuit voltages of the cells with various BZCY*y* (*y* = 0.0, 0.4 and 0.8) electrolytes.

$BaZr_{0.85}Y_{0.15}O_3$ proton-conducting electrolyte by Babilo and Haile [34].

3.4. Fuel cell performance

The fuel cell performance of the above mentioned anode-supported fuel cells was investigated by applying 3% H_2O humidified hydrogen as the fuel and ambient air as the cathode atmosphere. Fig. 6 shows the temperature dependences of the open circuit voltages (OCV) of the cells with different zirconium contents in the BZCY*y* electrolyte. High OCVs of around 1.10 V, near the theoretical values, were observed for the fuel cells with BZCY*y* electrolytes. This suggests that there was no serious leakage of the electrolyte membranes. This further supports the fact that the electrolyte layers were well densified and that the possible diffusion of nickel oxide into the electrolyte during the high temperature sintering did not have obvious effect on the transportation properties of the electrolyte on the other hand. The high OCVs of the fuel cell with the BZCY0.8 electrolyte imply that the electrolyte membrane was also well densified, although the sintering was low at 1450 °C. This agrees well with the SEM observations.

Although BSCF has been applied to many oxygen ion conducting electrolytes such as SDC, the application of BSCF on proton conductors is still rarely reported. Our primary results have shown the potential application of BSCF also for BCY electrolyte [3]. Fig. 7 shows the *I–V* curves of the cells that have the same cathode of BSCF but different BZCY*y* electrolytes. The linear response of the cell voltage to the applied polarization current density indicates that the concentration polarization did not occur for all fuel cells. It suggests that the electrodes are sufficient porous for the free diffusion of the gaseous reactants and reaction products, which is due to the low sintering temperature of the cells. For the fuel cell with the BCY electrolyte, a peak power density of ~550 mW cm^{-2} at 750 °C was achieved, which is among the best results reported in the previous works about H^+-SOFCs [3,12]. At 500 °C, a peak power density of 81 mW cm^{-2} was still obtained. With the increase of the zirconium content in the electrolyte, the cell performance decreased progressively. At *y* = 0.8, a peak power density of about 45 mW cm^{-2} was achieved at 700 °C, which was higher than that for the thick BZCY0.8 electrolyte-supported cell with Pt electrodes as reported previously [12]. A favorable power density of 220 mW cm^{-2} was obtained at 750 °C and 84 mW cm^{-2} at 450 °C for the cell with the BZCY0.4 electrolyte. In connection with the favorable chemical stability against the CO_2 atmosphere and the good sintering in the thin-film configuration, BZCY0.4 is a potential electrolyte material for intermediate-temperature SOFCs.

Fig. 8 is the impedance spectroscopy of the cells with BZCY0.4 electrolytes. The spectroscopy indicates that both the ohmic resistance and the electrode polarization resistance increased with the decrease of temperature, which accounts for the reduced cell performance. But the omhic resistance is still much larger than the electrode polarization resistance at high temperatures. Even at 450 °C, the ohmic resistance is more than twice that of the electrode. This suggests that a further reduction in the electrolyte membrane thickness could result in an obvious increase in the cell performance.

Based on the $BaCe_{0.4}Zr_{0.4}Y_{0.2}O_{3-\delta}$ protonic conductivity at 700 °C [12,20], the ohmic resistance of the 35 μm thick film are estimated to be ~0.38 Ω cm^2. The large difference in ohmic resistance

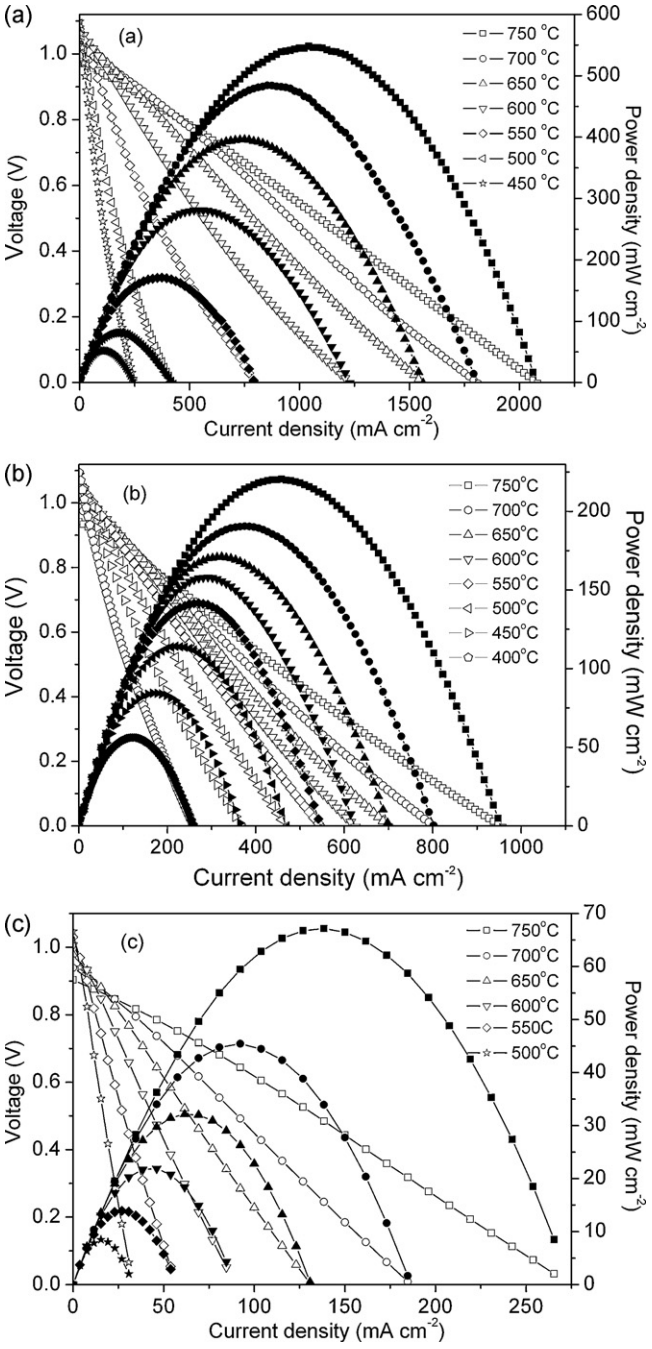

Fig. 7. *I–V* curves of the cells with various BZCY*y* electrolytes and the BSCF cathode: (a) *y* = 0.0; (b) *y* = 0.4; (c) *y* = 0.8.

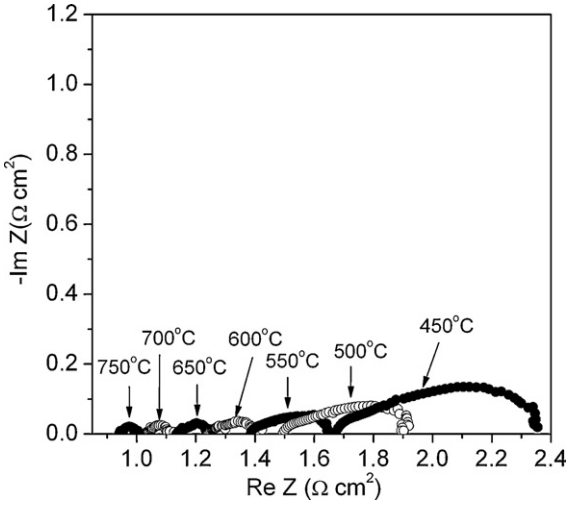

Fig. 8. The impedance spectroscopy of the cells under OCV conditions with BZCY0.4 electrolytes.

($\sim$1.02 $\Omega\,cm^2$) of the single cell is probably due to the additional contact resistance from the BSCF/BZCY0.4 interface and the Ni-BZCY0.4/BZCY0.4 interface as well as the wires. This may be the main reason for the poor cell performance even when the thin-film BZCY*y* electrolyte at high Zr content was adopted. It has been demonstrated that BSCF is not a good cathode for zirconium-based cells due to the serious interfacial reaction [35]. We have also demonstrated previously that the phase reaction between BSCF and BCY could form an interfacial layer with much lower conductivity than BCY, resulting in a significant decrease of the apparent electrolyte conductivity. The development of new cathode materials with high activity for oxygen reduction but negligible reactivity with BZCY electrolyte is then of significant importance for improving the cell performance of a fuel cell with heavily zirconium-doped BZCY*y* electrolyte.

4. Conclusions

The lattice constant and the sinterability of BZCY*y* decreased with increasing the Zr content while chemical stability against the CO_2 atmosphere increased. The perovskite structure of the BZCY*y* oxides was seriously destroyed as carbonate was formed at $y \leq 0.3$, but the main perovskite structure was survived at $y = 0.4$ and higher. The formative rate of carbonate was 8.70×10^{-7} mol m^{-2} min^{-1} at $y = 0.4$ while the formative rate of carbonate were 7.50×10^{-6} mol m^{-2} min^{-1} and only 7.00×10^{-8} mol m^{-2} min^{-1} at $y = 0.0$ and 0.8, respectively. The anode-supported configuration helped the sintering of the thin-film electrolyte. For a fuel cell with the BCY electrolyte, peak power density of about 550 and 81 mW cm^{-2} were obtained at 750 and 500 °C, respectively. With the increase of the zirconium content in the electrolyte, the cell performance decreased progressively. At $y = 0.8$, a peak power densities of approximately 45 and 8 mW cm^{-2} were achieved at 700 and 500 °C, respectively. However, a favorable power density of 220 mW cm^{-2} was obtained at 750 °C and 84 mW cm^{-2} was obtained at 450 °C for the cell with the BZCY0.4 electrolyte.

In order to further improve the H^+-SOFCs performance, increasing the relative density of $BaZr_yCe_{0.8-y}Y_{0.2}O_{3-\delta}$ ($0.0 \leq y \leq 0.8$) (BZCY*y*) with higher Zr doping content and increasing the sinterability by applying metal oxide as a sintering additives at lower temperature may be investigated. The development of new cathode materials with high activity for oxygen reduction but negligible reactivity with BZCY*y* electrolyte is also a significant future step.

Acknowledgements

This work was supported by the National Natural Science Foundation of China under contract Nos. 20703024, and 20676061, by the National 863 program under contract No. 2007AA05Z133, and by the National Basic Research Program of China under contract No. 2007CB209704.

References

[1] S.M. Haile, Acta Mater. 51 (2003) 5981–6000.
[2] B.C.H. Steele, J. Mater. Sci. 36 (2001) 1053–1068.
[3] Y. Lin, R. Ran, Y. Zheng, Z.P. Shao, W.Q. Jin, N.P. Xu, J. Ahn, J. Power Sources 180 (2008) 15–22.
[4] Z.P. Shao, S.M. Haile, Nature 431 (2004) 170–173.
[5] W. Zhou, Z.P. Shao, R. Ran, R. Cui, Electrochem. Commun. 10 (2008) 1647–1651.
[6] T. Ishihara, J.W. Yan, M. Shinagawa, H. Matsumoto, Electrochim. Acta 52 (2006) 1645–1650.
[7] B.C.H. Steele, A. Heinzel, Nature 414 (2001) 345–352.
[8] J.D. Solier, M.A. Pérez-Jubindo, A. Dominguez-Rodriguez, A.H. Heuer, J. Am. Ceram. Soc. 72 (1989) 1500–1502.
[9] T. Hibino, A. Hashimoto, M. Suzuki, M. Sano, J. Electrochem. Soc. 149 (2002) A1503–A1508.
[10] H. Iwahara, T. Esaka, H. Uchida, N. Maeda, Solid State Ionics 3–4 (1981) 359–363.
[11] H. Uchida, N. Maeda, H. Iwahara, Solid State Ionics 11 (1983) 117–124.
[12] E. Fabbri, A. D'Epifanio, E.D. Bartolomeo, S. Licoccia, E. Traversa, Solid State Ionics 179 (2008) 558–564.
[13] N. Maffei, L. Pelletier, A. McFarlan, J. Power Sources 136 (2004) 24–29.
[14] K.D. Kreuer, Annu. Rev. Mater. Res. 33 (2003) 333–359.
[15] M. Ni, M.K.H. Leung, D.Y.C. Leung, Int. J. Hydrogen Energy 33 (2008) 2337–2354.
[16] H. Iwahara, Solid State Ionics 86–88 (1996) 9–15.
[17] H. Matsumoto, Y. Kawasaki, N. Ito, M. Enoki, T. Ishihara, Electrochem. Solid State Lett. 10 (2007) B77–80.
[18] K. Xie, R.Q. Yan, X.R. Chen, S.L. Wang, Y.Z. Jiang, X.Q. Liu, G.Y. Meng, J. Alloys Compd. 473 (2009) 323–329.
[19] C.D. Zuo, S.W. Zha, M.L. Liu, M. Hatano, M. Uchiyama, Adv. Mater. 18 (2006) 3318–3320.
[20] K. Katahira, Y. Kohchi, T. Shimura, H. Iwahara, Solid State Ionics 138 (2000) 91–98.
[21] K.H. Ryu, S.M. Haile, Solid State Ionics 125 (1999) 355–367.
[22] S.V. Bhide, A.V. Virkar, J. Electrochem. Soc. 146 (1999) 2038–2044.
[23] Z.M. Zhong, Solid State Ionics 178 (2007) 213–220.
[24] L. Bi, S.Q. Zhang, S.M. Fang, Z.T. Tao, R.R. Peng, W. Liu, Electrochem. Commun. 10 (2008) 1598–1601.
[25] S. Barison, M. Battagliarin, T. Cavallin, L. Doubova, M. Fabrizio, C. Mortaliò, S. Boldrini, L. Malavast, R. Gerbasi, J. Mater. Chem. 18 (2008) 5120–5128.
[26] B. Lin, M.J. Hu, J.J. Ma, Y.Z. Jiang, S.W. Tao, G.Y. Meng, J. Power Sources 183 (2008) 479–484.
[27] J.D. Lv, L. Wang, D. Lei, H.X. Guo, R.V. Kumar, J. Alloys Compd. 467 (2009) 376–382.
[28] A.K. Azad, J.T.S. Irvine, Solid State Ionics 178 (2007) 635–640.
[29] A. D'Epifanio, E. Fabbri, E. Di Bartolomeo, S. Licoccia, E. Traversa, Fuel Cells 8 (2008) 69–76.
[30] K.D. Kreuer, Solid State Ionics 125 (1999) 285–302.
[31] S.M. Haile, G. Staneff, K.H. Ryu, J. Mater. Sci. 36 (2001) 1149–1160.
[32] S.W. Tao, J.T.S. Irvine, J. Solid State Chem. 180 (2007) 3493–3503.
[33] S.W. Tao, J.T.S. Irvine, Adv. Mater. 18 (2006) 1581–1584.
[34] P. Babilo, S.M. Haile, J. Am. Ceram. Soc. 88 (2005) 2362–2368.
[35] Q.S. Zhu, T.A. Jin, Y. Wang, Solid State Ionics 177 (2006) 1199–1204.